Finite-bandwidth effects on the causal prediction of ultrasonic attenuation of the power-law form

Joel Mobley
Oak Ridge National Laboratory, P.O. Box 2008, Oak Ridge, Tennessee 37831-6101

Kendall R. Waters and James G. Miller [a)]
Laboratory for Ultrasonics, Washington University in St. Louis, St. Louis, Missouri 63130

(Received 16 August 2002; revised 13 August 2003; accepted 2 September 2003)

Kramers–Kronig (K–K) relations exist as a consequence of causality, placing nonlocal constraints on the relationship between dispersion and absorption. The finite-bandwidth method of applying these relations is examined where the K–K integrals are restricted to the spectrum of the experimental data. These finite-bandwidth K–K relations are known to work with resonant-type data and here are applied to dispersion data consistent with a power-law attenuation coefficient (exponent from 1 to 2). Bandwidth-restricted forms of the zero and once-subtracted K–K relations are used to determine the attenuation coefficient from phase velocity. Analytically, it is shown that these transforms produce the proper power-law form of the attenuation coefficient as a stand-alone term summed with artifacts that are dependent on the integration limits. Calculations are performed to demonstrate how these finite-bandwidth artifacts affect the K–K predictions under a variety of conditions. The predictions are studied in a local context as a function of subtraction frequency, bandwidth, and power-law exponent. The K–K predictions of the power-law exponent within various decades of the spectrum are also examined. In general, the agreement between finite-bandwidth K–K predictions and exact values grows as the power-law exponent approaches 1 and with increasing bandwidth.
[DOI: 10.1121/1.1621394]

PACS numbers: 43.35.Bf, 43.35.Cg, 43.20.Hq [RLW]

Pages: 2782–2790

I. INTRODUCTION

Fundamentally rooted in causality, Kramers–Kronig (K–K) relations have proven to be powerful, practical tools with applications across many disciplines of physics. In ultrasonics, subtracted forms of the K–K relations have been used to accurately predict dispersion and attenuation in systems exhibiting resonant behavior (encapsulated microbubbles[1]) and power-law growth[2] in attenuation. The principal difficulty in applying K–K relations directly to ultrasonic data is the finite bandwidth inherent in experimentally measured spectra. By restricting the range of integration to the measurement spectrum, artifacts are introduced that can seriously impact the accuracy of K–K transformations. It is still an open question as to whether an accurate general procedure exists for applying K–K relations directly (i.e., blindly) to any type of dispersion/attenuation data, or if some information (e.g., an analytical model) about the target system beyond the bandlimited attenuation and dispersion data is required to overcome the artifacts.

Previously, we examined the finite-bandwidth K–K problem for resonant systems using experimental data from Albunex® microbubble suspensions. Within the measurement spectrum, which covered more than a decade in frequency, these data exhibited a single, well-resolved resonance with a full-width at half maximum covering about one quarter of the total bandwidth. For such a system, we found that accurate K–K inversions were possible using only the measured dispersion and attenuation data (i.e., no out-of-band extrapolations or model fitting were required). In contrast, this work focuses on the systems that exhibit monotonic dispersion and attenuation, specifically those whose attenuation coefficient can be described by a power law. The power-law form of the attenuation coefficient is consistent with the behavior of a considerable number of solids,[3] liquids,[2,3] and biological tissues[4,5] in the MHz range, and is thus of interest in ultrasonic research. An accurate model-dependent procedure for applying K–K transformations specifically to power-law systems has been demonstrated previously.[2] In that study, the data were fit to the power-law model, and the predictions are expressed as functions of the fitting parameters. These expressions for velocity and attenuation are derived by assuming the model used to fit the data can be extrapolated to the entire spectrum, from $\omega=0$ to $\omega\to\infty$. The present study is distinguished from this earlier work because here we assume that the model holds only within the bandwidth of interest, and we examine the impact this spectrally limited knowledge imposes on K–K predictions. This paper is specifically concerned with calculating the attenuation coefficient with finite-bandwidth K–K using the causally consistent form of the phase velocity as the input.

There are two aspects of the finite-bandwidth K–K problem that are specifically addressed in this work. The first part of the study examines the case where a subtraction frequency ω_0 is chosen at an interior frequency well within the bandwidth of interest (at least a factor of 2 above the lower limit). This portion of the study is a test of the K–K calculation procedure that was successfully applied to the resonant

a)Electronic mail: james.g.miller@wustl.edu

microbubble data,[1] where certain choices of ω_0 across the spectrum optimized the accuracy of the predictions. This part also has implications for composite media that have both resonant and power-law features (e.g., particles suspended in an oil). The second part of the study is concerned with predicting the power-law exponent of the attenuation coefficient from the K–K transformation of bandlimited dispersion data. In this case, both the subtraction frequency and lower limit of integration are taken to be zero. The power-law trajectory of the K–K predicted attenuation coefficient is examined in individual decades of frequency (i.e., powers of 10) below and up to the upper limit of integration.

In Sec. II, we provide some background on the transfer characteristics of media with a power-law attenuation coefficient and the causally consistent form for the phase velocity. The finite-bandwidth forms of the subtracted Kramers–Kronig relations are also introduced. In Sec. III analytical expressions for the finite-bandwidth K–K predictions of the attenuation coefficient are given. These results are the sum of two terms, the first being the proper power-law result and the second encompassing the finite-bandwidth artifact. In Sec. IV, the analytical results from Sec. III are used to calculate attenuation coefficient curves under various circumstances. The discussions of these results are woven throughout Sec. IV.

II. BACKGROUND

A. Ultrasonic attenuation and dispersion in power-law systems

The linear transport of ultrasonic waves across an isotropic medium of thickness D is accounted for in general by a Fourier-domain transfer function of the form

$$H(\omega,D)=\exp[iK(\omega)D], \tag{1}$$

where $K(\omega)=[\omega/c(\omega)]+i\alpha(\omega)$ is the complex wave number, $\alpha(\omega)$ is the attenuation coefficient, and $c(\omega)$ is the phase velocity. Experimentally, a power-law form of the attenuation coefficient

$$\alpha(\omega)=\alpha_0\omega^{1+\varepsilon} \quad \text{where} \quad 0\leqslant\varepsilon\leqslant 1, \tag{2}$$

has been found to provide an accurate fit to broadband data from a variety of solid and liquid materials within the respective measurement bandwidths. When Eq. (2) holds for the entire frequency spectrum, the phase velocity takes the causally consistent form[2,3]

$$\frac{1}{c(\omega)}-\frac{1}{c(\omega_0)}=\alpha_0\tan\left[(1+\varepsilon)\frac{\pi}{2}\right](\omega^{\varepsilon}-\omega_0^{\varepsilon}) \quad 0<\varepsilon\leqslant 1 \tag{3a}$$

and

$$=-\alpha_0\frac{2}{\pi}\ln\frac{\omega}{\omega_0} \quad \varepsilon=0. \tag{3b}$$

[Equation (3b) can be obtained by taking the $\varepsilon\to 0$ limit of Eq. (3a).] This form of the dispersion as well as the consistency of Eq. (2) and Eq. (3) have also been verified in the laboratory.[2,3] [Both $\alpha(\omega)$ and $c(\omega)$ are even functions, a property derived from the fact that $H(\omega,D)$ is the Fourier transform of a real function. Since negative frequencies are not explicitly considered, no absolute value signs are used.]

B. Kramers–Kronig relations for ultrasonic attenuation and phase velocity

Given that the medium described by $H(\omega,D)$ satisfies the physical requirements of causality and finite energy, the real and imaginary parts of $H(\omega,D)$ can be shown to form a Hilbert transform pair via Titchmarsh's theorem. The integration over negative frequencies can be mapped to the positive axis, and the resulting expressions are commonly known as Kramers–Kronig relations. The complex wave number itself derives its analytic properties from the transfer function, and under the proper conditions the complex wave number will retain the domain of analyticity required of Hilbert transform pairs. However, it will not fulfill the square integrability requirements since the attenuation coefficient must diverge as $\omega\to\infty$ to insure the square integrability of $H(\omega,D)$. In spite of this, K–K relations between $\alpha(\omega)$ and $c(\omega)$ can be derived by the method of subtractions,[6] which insures convergence of the integrals. Formed using $\gamma(\omega)=iK(\omega)$ as the basis function, the unsubtracted and once-subtracted relations are considered here. To allow for the straightforward adaptation to the restricted interval case, the relations are given in their expanded form.[1] The unsubtracted (zeroth) relation for the attenuation coefficient is

$$\alpha(\omega)=\lim_{\substack{\Omega\to\infty\\ \sigma\to 0}}\left[-\frac{1}{\pi}\int_{\sigma}^{\Omega}\frac{\dfrac{\omega'}{c(\omega')}-\dfrac{\omega}{c(\omega)}}{\omega'-\omega}d\omega'-\frac{1}{\pi}\int_{\sigma}^{\Omega}\frac{\dfrac{\omega'}{c(\omega')}+\dfrac{\omega}{c(\omega)}}{\omega'+\omega}d\omega'\right]. \tag{4}$$

Combining the two integrands into a single rational expression and counting the powers of ω', one can see that convergence requires that $\varepsilon<-1$ [where $\omega'/c(\omega')\sim\omega'^{1+\varepsilon}$]. This is, of course, inadequate for the range of power laws considered here, and higher-order subtractions must be considered. The once-subtracted relation in the expanded form is

$$\alpha(\omega)=\alpha(\omega_0)+\lim_{\substack{\Omega\to\infty\\ \sigma\to 0}}\left[-\frac{1}{\pi}\int_{\sigma}^{\Omega}\frac{\dfrac{\omega'}{c(\omega')}-\dfrac{\omega}{c(\omega)}}{\omega'-\omega}d\omega'-\frac{1}{\pi}\int_{\sigma}^{\Omega}\frac{\dfrac{\omega'}{c(\omega')}+\dfrac{\omega}{c(\omega)}}{\omega'+\omega}d\omega'+\frac{1}{\pi}\int_{\sigma}^{\Omega}\frac{\dfrac{\omega'}{c(\omega')}-\dfrac{\omega_0}{c(\omega_0)}}{\omega'-\omega_0}d\omega'+\frac{1}{\pi}\int_{\sigma}^{\Omega}\frac{\dfrac{\omega'}{c(\omega')}+\dfrac{\omega_0}{c(\omega_0)}}{\omega'+\omega_0}d\omega'\right], \tag{5}$$

where ω_0 is referred to as the subtraction frequency. By counting the powers of ω' after combining all four integrands, one can expect convergence for $\varepsilon<1$ which covers the range of power laws examined in this work. Note that for $\varepsilon=1$, there is no dispersion so this case is naturally excluded. We will refer to these K–K expressions whose integrals cover the entire positive frequency axis [i.e., $(\sigma,\Omega)\to(0,\infty)$] as "unrestricted."

The interval-restricted (i.e., finite-bandwidth) relations are given by

$$\alpha(\omega)^{(\sigma,\Omega,n=0)}=-\frac{1}{\pi}\int_\sigma^\Omega\frac{\frac{\omega'}{c(\omega')}-\frac{\omega}{c(\omega)}}{\omega'-\omega}d\omega'-\frac{1}{\pi}\int_\sigma^\Omega\frac{\frac{\omega'}{c(\omega')}+\frac{\omega}{c(\omega)}}{\omega'+\omega}d\omega', \tag{6}$$

and

$$\alpha(\omega)^{(\sigma,\Omega,n=1)}=\alpha(\omega_0)-\frac{1}{\pi}\int_\sigma^\Omega\frac{\frac{\omega'}{c(\omega')}-\frac{\omega}{c(\omega)}}{\omega'-\omega}d\omega'-\frac{1}{\pi}\int_\sigma^\Omega\frac{\frac{\omega'}{c(\omega')}+\frac{\omega}{c(\omega)}}{\omega'+\omega}d\omega'+\frac{1}{\pi}\int_\sigma^\Omega\frac{\frac{\omega'}{c(\omega')}-\frac{\omega_0}{c(\omega_0)}}{\omega'-\omega_0}d\omega'+\frac{1}{\pi}\int_\sigma^\Omega\frac{\frac{\omega'}{c(\omega')}+\frac{\omega_0}{c(\omega_0)}}{\omega'+\omega_0}d\omega', \tag{7}$$

where n is the subtraction order and the limits of integration are such that $0\leqslant\sigma<\Omega$.

III. THEORY

The results shown in this section are calculated by substituting the dispersion as given in Eq. (3a) and Eq. (3b) into the restricted interval forms, Eq. (6) and Eq. (7). The forms of the restricted K–K results depend on whether or not the evaluation frequency, ω, and the subtraction frequency, ω_0, are contained within the integration interval. The viewpoint taken in this work is that the bandwidth of integration denotes the extent of our knowledge about the complex wave number, and thus we examine only the situation where $\sigma<\omega$, $\omega_0<\Omega$. In all cases considered, $0\leqslant\varepsilon<1$. From the unsubtracted relation [Eq. (6)]

$$\alpha(\omega)^{(\sigma,\Omega,0)}=\alpha_0\omega^{1+\varepsilon}+F_0^{(\omega)}(\sigma,\Omega), \tag{8}$$

where $F_0^{(\omega)}(\sigma,\Omega)$ represents the artifactual terms that explicitly depend on the limits of integration

$$F_0^{(\omega)}(\sigma,\Omega)=-\frac{2}{\pi}\frac{\Omega-\sigma}{c(\omega)}-\frac{\alpha_0}{\pi}\tan\left[(1+\varepsilon)\frac{\pi}{2}\right]\times\left(2\sigma^{1+\varepsilon}\sum_{n=0}^{\infty}\frac{1}{2n+\varepsilon+3}\frac{\sigma^{2n+2}}{\omega^{2n+2}}-2\Omega^{1+\varepsilon}\sum_{n=0}^{\infty}\frac{1}{2n-\varepsilon-1}\frac{\omega^{2n}}{\Omega^{2n}}-2(\Omega-\sigma)\omega^{\varepsilon}-\omega^{1+\varepsilon}\ln\frac{\omega+\sigma}{\omega-\sigma}\frac{\Omega-\omega}{\Omega+\omega}\right) \tag{9a}$$

$$=-\frac{2}{\pi}\frac{\Omega-\sigma}{c(0)}-\frac{\alpha_0}{\pi}\tan\left[(1+\varepsilon)\frac{\pi}{2}\right]\times\left(2\sigma^{1+\varepsilon}\sum_{n=0}^{\infty}\frac{1}{2n+\varepsilon+3}\frac{\sigma^{2n+2}}{\omega^{2n+2}}-2\Omega^{1+\varepsilon}\sum_{n=0}^{\infty}\frac{1}{2n-\varepsilon-1}\frac{\omega^{2n}}{\Omega^{2n}}-\omega^{1+\varepsilon}\ln\frac{\omega+\sigma}{\omega-\sigma}\frac{\Omega-\omega}{\Omega+\omega}\right). \tag{9b}$$

In the limit of $\varepsilon\to0$ (logarithmic dispersion), the remainder becomes

$$\lim_{\varepsilon\to0}F_0^{(\omega)}(\sigma,\Omega)=-\frac{2}{\pi}\left(\frac{\Omega}{c(\Omega)}-\frac{\sigma}{c(\sigma)}\right)+\frac{2\alpha_0\omega}{\pi^2}\left(\ln\frac{\sigma}{\omega}\ln\frac{\omega+\sigma}{\omega-\sigma}-\ln\frac{\Omega}{\omega}\ln\frac{\Omega+\omega}{\Omega-\omega}-2\sum_{n=0}^{\infty}\frac{1}{(2n+3)^2}\frac{\sigma^{2n+3}}{\omega^{2n+3}}-2\sum_{n=0}^{\infty}\frac{1}{(2n-1)^2}\frac{\omega^{2n-1}}{\Omega^{2n-1}}\right). \tag{10}$$

In the limits $\sigma\to0$ and $\Omega\gg\omega$, this becomes

$$\alpha(\omega)^{(0,\Omega\gg\omega,0)}=\alpha_0\omega^{1+\varepsilon}-\Omega^{1+\varepsilon}\frac{2}{1+\varepsilon}\frac{\alpha_0}{\pi}\tan\left[(1+\varepsilon)\frac{\pi}{2}\right]\quad 0<\varepsilon<1 \tag{11a}$$

$$=\alpha_0\omega^{1+\varepsilon}-\Omega\frac{2}{\pi}\left(\frac{1}{c(\Omega)}+\frac{2\alpha_0}{\pi}\right)\quad\varepsilon=0, \tag{11b}$$

which diverges as $\Omega\to\infty$ as anticipated.

The relation with one subtraction yields the following:

$$\alpha(\omega)^{(\sigma,\Omega,1)}=\alpha_0\omega^{1+\varepsilon}-\alpha_0\omega_0^{1+\varepsilon}+\alpha(\omega_0)+F_1^{(\omega,\omega_0)}(\sigma,\Omega) \tag{12a}$$

$$=\alpha_0\omega^{1+\varepsilon}+F_1^{(\omega,\omega_0)}(\sigma,\Omega), \tag{12b}$$

where

$$F_1^{(\omega,\omega_0)}(\sigma,\Omega) = -\frac{\alpha_0}{\pi}\tan\left[(1+\varepsilon)\frac{\pi}{2}\right] \times\left(2\sigma^{1+\varepsilon}\sum_{n=0}^{\infty}\frac{\sigma^{2n+2}}{2n+\varepsilon+3}\left(\frac{1}{\omega^{2n+2}}-\frac{1}{\omega_0^{2n+2}}\right) -2\Omega^{1+\varepsilon}\sum_{n=1}^{\infty}\frac{1}{2n-\varepsilon-1}\frac{\omega^{2n}-\omega_0^{2n}}{\Omega^{2n}} -\omega^{1+\varepsilon}\ln\frac{\omega+\sigma}{\omega-\sigma}\frac{\Omega-\omega}{\Omega+\omega}+\omega_0^{1+\varepsilon}\ln\frac{\omega_0+\sigma}{\omega_0-\sigma}\frac{\Omega-\omega_0}{\Omega+\omega_0}\right). \tag{13}$$

In the limit $\varepsilon\to 0$, the remainder term becomes

$$\lim_{\varepsilon\to 0} F_1^{(\omega,\omega_0)}(\sigma,\Omega) = \frac{2\alpha_0}{\pi^2}\left(\omega\ln\frac{\sigma}{\omega}\ln\frac{\omega+\sigma}{\omega-\sigma}-\omega_0\ln\frac{\sigma}{\omega_0}\ln\frac{\omega_0+\sigma}{\omega_0-\sigma} -\omega\ln\frac{\Omega}{\omega}\ln\frac{\Omega+\omega}{\Omega-\omega}+\omega_0\ln\frac{\Omega}{\omega_0}\ln\frac{\Omega+\omega_0}{\Omega-\omega_0} -2\sigma\sum_{n=0}^{\infty}\frac{\sigma^{2n+2}}{(2n+3)^2}\left(\frac{1}{\omega^{2n+2}}-\frac{1}{\omega_0^{2n+2}}\right) -2\Omega\sum_{n=0}^{\infty}\frac{1}{(2n-1)^2}\frac{\omega^{2n}-\omega_0^{2n}}{\Omega^{2n}}\right). \tag{14}$$

Taking the limit of large Ω and small σ

$$\lim_{\Omega\gg\omega,\omega_0}\alpha(\omega)^{(\sigma,\Omega,1)} = \alpha_0\omega^{1+\varepsilon}+\frac{\alpha_0}{\pi}\tan\left[(1+\varepsilon)\frac{\pi}{2}\right]\frac{2}{1-\varepsilon}\frac{\omega^2-\omega_0^2}{\Omega^{1-\varepsilon}} \quad 0<\varepsilon<1 \tag{15a}$$

$$= \alpha_0\omega-\frac{4\alpha_0}{\pi^2}\frac{\omega^2-\omega_0^2}{\Omega} \quad \varepsilon=0, \tag{15b}$$

which converge to $\alpha(\omega)$ in the limit of $\Omega\to\infty$. The subtraction frequency ω_0 exerts no influence on the shape of $\alpha(\omega)^{(\sigma,\Omega,1)}$, but only serves to "anchor" $\alpha(\omega)^{(\sigma,\Omega,1)}$ to $\alpha(\omega)$ at $\omega=\omega_0$. To confirm these analytical results, the restricted bandwidth relation of Eq. (7) was numerically integrated under a variety of conditions using the form of the dispersion in Eq. (3a). In all of these comparisons, the analytical expression and numerical integrations produced essentially equivalent outcomes.

Both the zeroth- and first-order calculations produce results with the same general structure—the correct power-law form of the attenuation coefficient coexisting with additional additive terms that depend upon at least one of the limits of integration. However, in the unsubtracted result the extra terms grow with increasing Ω, while the once-subtracted result converges to the correct result as $\Omega\to\infty$.

IV. RESULTS AND DISCUSSION

A. Locally anchored performance ($\omega_0 \geqslant 2\sigma$)

The unrestricted K–K relations have demonstrated their utility for power-law systems, since they generate analytical forms for the attenuation and dispersion [Eq. (2) and Eq. (3)] that are consistent with experimental data.[2] In this model-dependent approach the K–K inversion is reduced to the simple act of determining α_0 and ε through some fitting procedure. Even though the model-fitting method has so far proven a successful approach for performing K–K transformations of power-law systems, there are two principal reasons for investigating their behavior with the more general restricted-bandwidth K–K. First, the restricted K–K method has been shown to work for resonant-type data without using any model-dependent or extrapolated parameters.[1] It is then natural to investigate the method with other types of data to assess its wider applicability. Second, it is possible to have a system that has a combination of localized resonant structures riding on a power-law background. Since many liquids exhibit power-law attenuation, suspensions of microbubbles or microspheres in such a liquid could display this composite behavior.

As shown in the previous study of the microbubble system, the accuracy of the restricted K–K prediction for an isolated resonance comes down to the choice of the subtraction frequency ω_0. Certain choices of ω_0 from within the data spectrum effectively minimize the finite-bandwidth artifacts, and the rationale behind these choices was demonstrated using an analytical model.[1] For the present power-law case, the accuracy of the restricted-bandwidth approach has more to do with the bandwidth of the data than the choice of subtraction frequency. The results shown in this section (see Fig. 1) are meant to examine the restricted K–K approach in a manner consistent with the way they are applied to the resonant data; specifically the subtraction frequency is chosen from the known bandwidth and is distinct from the band edges. Also, the limits of integration include realistic measurement bandwidths.

In Fig. 1 the restricted K–K predictions, calculated using Eq. (12), are plotted over a region around the subtraction frequency ω_0 for various limits of integration. The region of the spectrum displayed in the figure (from $0.5\omega_0$ to $1.5\omega_0$) shows only a portion of the total spectra used to calculate the four K–K curves. This spectral region displayed in Fig. 1 encompasses the widths of resonant peaks encountered in data from encapsulated microbubble[1] ($\omega_{\text{res}}/\Delta\omega^{\text{full width}}_{\text{half max}}\sim 1$) and polymer microsphere[7] ($\omega_{\text{res}}/\Delta\omega^{\text{full width}}_{\text{half max}}\sim 10$) suspensions. This serves to illustrate the behavior of the predicted curves over those frequency scales encountered in resonant data with resolved peaks. In panel (a), the $1+\varepsilon=1.1$ results are plotted. For the curve calculated using the widest bandwidth (with lower limit of integration $\sigma=0.05\omega_0$, and upper limit of integration $\Omega=50\omega_0$), the K–K prediction accounts for 89% of the variation in the exact curve. If the lower limit

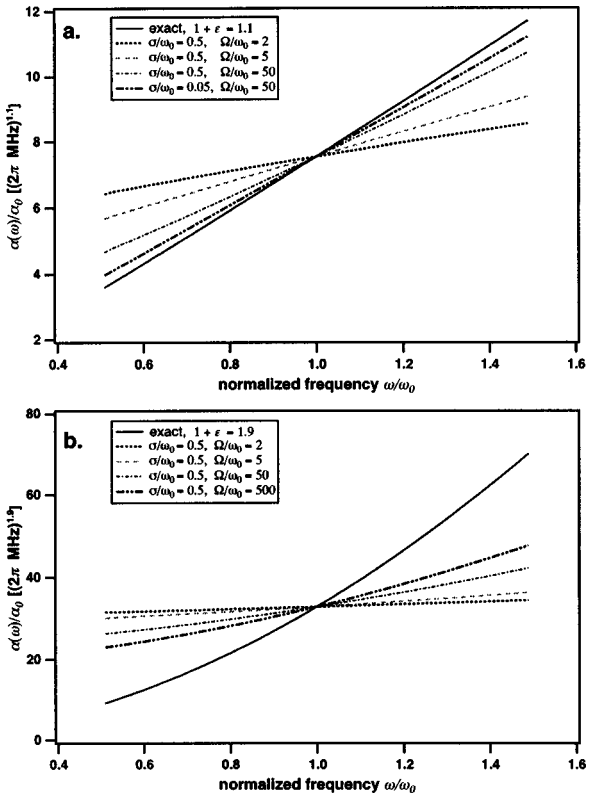

FIG. 1. (a) The comparison of $\alpha(\omega)^{(\sigma,\Omega,1)}$ and $\alpha(\omega)$ for $1+\varepsilon=1.1$ around the subtraction frequency ω_0 for bandwidths indicated in the legends. (b) Comparison of $\alpha(\omega)^{(\sigma,\Omega,1)}$ and $\alpha(\omega)$ for $1+\varepsilon=1.9$.

of integration is moved up to the boundary of the plotted curves ($\sigma=0.5\omega_0$) while holding the upper limit fixed, the predicted variation falls to 75% of the target value. The predicted variation decreases further as the upper limit is lowered, down to 26% of the exact value for the narrowest bandwidth case, $\sigma=0.5\omega_0$ to $\Omega=2\omega_0$. In panel (b), the $1+\varepsilon=1.9$ results are shown. Here, the predictions are relatively insensitive to changes in σ, so the only changes from curve to curve are in Ω. In this case the predicted variations in the attenuation coefficient range from 41% down to 5% of the exact value. The impact of these results on predicting peaks and trends ultimately depends on many system-dependent factors (e.g., relative peak-to-background ratio). When the peak is localized above (below) the subtraction frequency, the peak-to-background ratio will be over (under) estimated. If the resonant peaks are clearly resolved, when the peak is near ω_0 it can be reproduced without significant distortion, especially for the smaller values of ε. In fact, the restricted K–K transform is like a ''local filter'' in this case, suppressing the monotonic global trend in favor of the localized variations.

B. Predicted power-law trajectories, ω_0, $\sigma\rightarrow 0$

In this section, we apply the restricted K–K relations in a manner suited to predicting power-law exponents for the attenuation coefficient. For this purpose, the spectrum will be examined in specific decades (i.e., powers of 10) down from the upper limit of integration. In each decade, a power law is fit to the predicted curve to estimate the exponent for the curve. The subtraction frequency and lower limit of integration are taken to be equal and arbitrarily close to zero so that all terms containing σ and ω_0 as factors vanish. The once-subtracted results for $\alpha(\omega)^{(\sigma,\Omega,1)}$, expressed in Eq. (12), are calculated for four power laws, $1+\varepsilon=1.9$, 1.5, 1.1, and 1.0 (logarithmic dispersion). The objective is to identify the regions of the spectrum in which there is agreement between the predicted and exact power-law exponents. In all of the results to follow (shown in Figs. 2–5), the power-law fits to $\alpha(\omega)^{(\sigma,\Omega,1)}$ have an R^2 value $\geqslant 0.99$.

The results of the $1+\varepsilon=1.0$ case, where the dispersion is logarithmic, are shown in Fig. 2. In panel (a), $\alpha(\omega)^{(\sigma,\Omega,1)}$ and $\alpha(\omega)$ are compared on a log–log plot covering three decades in frequency up to the upper limit of integration Ω. One can see that the prediction tracks the exact trajectory well for $\omega/\Omega<0.05$. In panel (b), $\alpha(\omega)^{(\sigma,\Omega,1)}$ and $\alpha(\omega)$ are compared on a linear–linear plot over the range $0.001<\omega/\Omega\leqslant 0.01$, two decades down from the upper limit. A power-law fit to $\alpha(\omega)^{(\sigma,\Omega,1)}$ for just this decade yields $1+\varepsilon=0.99$. In panel (c), $\alpha(\omega)^{(\sigma,\Omega,1)}$ and $\alpha(\omega)$ are compared over the top decade, $0.1<\omega/\Omega\leqslant 1$, where a power-law fit to $\alpha(\omega)^{(\sigma,\Omega,1)}$ yields $1+\varepsilon=0.77$. Thus, to match the proper power-law trajectory with restricted K–K to about 1% in this case requires knowledge of the dispersion about 1.5 orders of magnitude above the frequency scale of interest.

The five panels of Fig. 3 display the results for the $1+\varepsilon=1.1$ case. In this figure (and the ones to follow) in addition to $\alpha(\omega)^{(\sigma,\Omega,1)}$ and $\alpha(\omega)$, we also plot the dominant artifactual terms from Eq. (12). For the cases examined here where ω_0 and σ are arbitrarily small, the artifact is due to two terms—referred to as the ''Ω series''

$$\frac{\alpha_0}{\pi}\tan\left[(1+\varepsilon)\frac{\pi}{2}\right]2\Omega^{1+\varepsilon}\sum_{n=1}^{\infty}\frac{1}{2n-\varepsilon-1}\frac{\omega^{2n}}{\Omega^{2n}}, \tag{16}$$

and the ''log term''

$$\frac{\alpha_0}{\pi}\tan\left[(1+\varepsilon)\frac{\pi}{2}\right]\omega^{1+\varepsilon}\ln\frac{1-\omega/\Omega}{1+\omega/\Omega}. \tag{17}$$

In panel (a), the quantities $\alpha(\omega)^{(\sigma,\Omega,1)}$ and $\alpha(\omega)$ are shown on a log–log plot covering three decades of the spectrum up to Ω. Moving down the frequency scale, the two curves merge in the middle decade similar to the previous case. In panel (b), $\alpha(\omega)^{(\sigma,\Omega,1)}$ and $\alpha(\omega)$ are compared on a linear plot over the third decade down from Ω. Here, the fit to $\alpha(\omega)^{(\sigma,\Omega,1)}$ yields an exponent of $1+\varepsilon=1.09$, demonstrating the high degree of agreement at this scale. In panel (c), the two quantities comprising the error are plotted over the same decade as panel (b). The two terms act in opposition to one another, with the Ω series having the greater magnitude. Note that the scale of the y axis in panel (c) is an order of magnitude smaller than that of panel (b). In panel (d), the exact and predicted K–K results are plotted for the top decade, and the deviation between the two is clear. A power-law fit over this decade produces $1+\varepsilon=0.86$. This is 78% of the target value, very similar to the previous case in the top decade. In panel (e) the error terms are shown to have similar shapes and are largely counterbalancing one another. Also

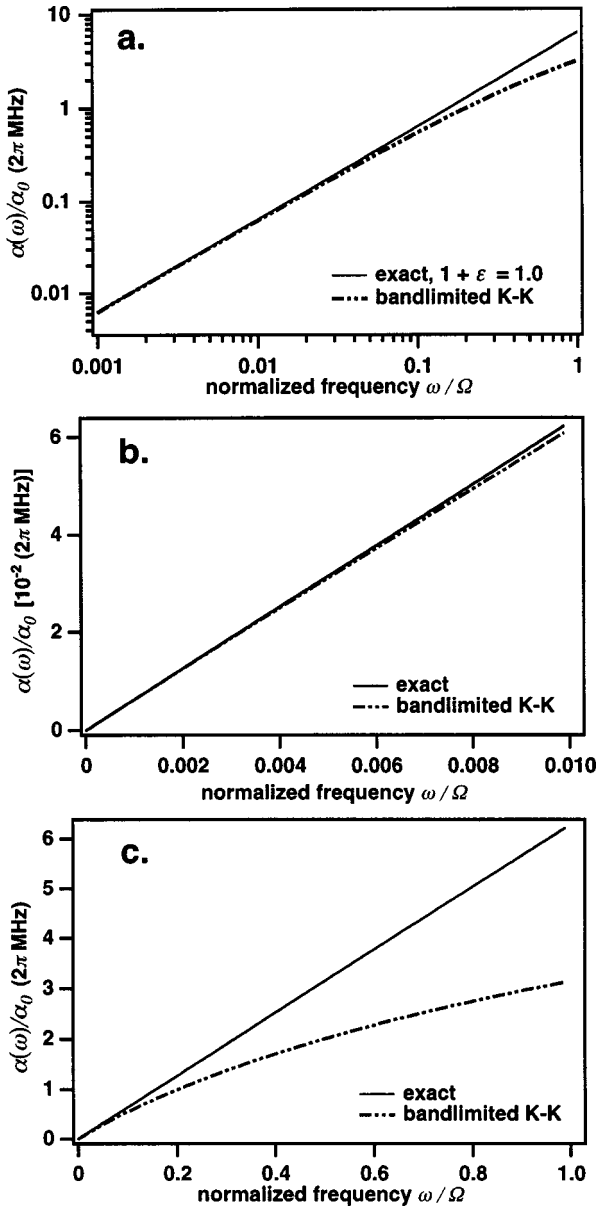

FIG. 2. (a) Log–log plot of the exact and restricted-interval once-subtracted K–K prediction for attenuation coefficient for $1+\varepsilon=1.0$, the logarithmic dispersion case, covering three decades in frequency. (b) A linear plot of the exact and predicted attenuation coefficients for the third decade, $0.001<\omega/\Omega\leqslant 0.01$. (c) A linear plot of the exact and predicted attenuation coefficient over the top decade ($\omega/\Omega<1.0$).

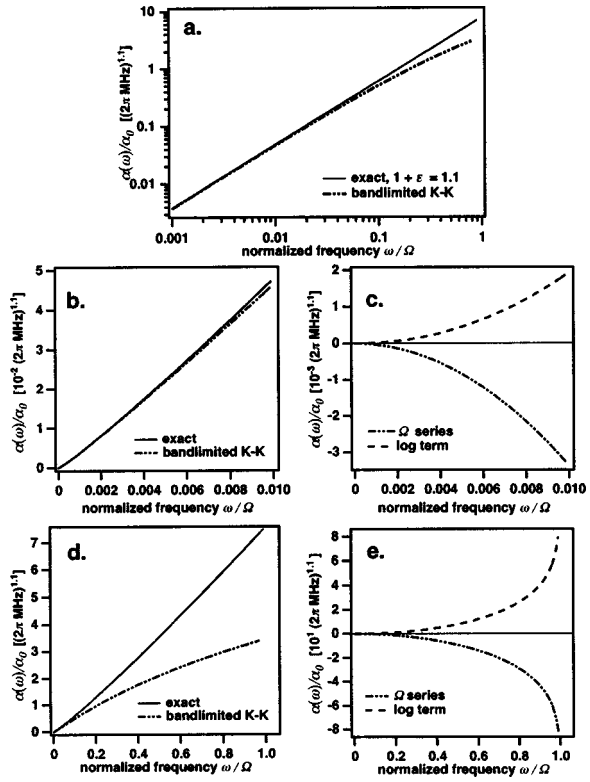

FIG. 3. (a) Log–log plot of the exact and restricted-interval once-subtracted K–K prediction for attenuation coefficient for $1+\varepsilon=1.1$. The plot covers three decades in frequency. (b) A linear plot of the exact and predicted attenuation coefficients over the third decade, $0.001<\omega/\Omega\leqslant 0.01$. (c) The two error terms, the Ω series [Eq. (16)] and the log term [Eq. (17)], in the K–K calculations for the third decade. The vertical scale is an order of magnitude narrower than that in panel (b). (d) A linear plot of the exact and predicted attenuation coefficient over the top decade ($\omega/\Omega<1.0$). (e) The two error terms in the K–K calculations for the top decade. Here, the vertical axis is 20 times broader than that of panel (d).

note that the two error terms are individually much larger than $\alpha(\omega)^{(\sigma,\Omega,1)}$ and $\alpha(\omega)$, as the vertical axis is about 20 times broader than in panel (d). Both error terms individually diverge in the $\omega\rightarrow\Omega$ limit, but one can show that together these divergences cancel.

Figure 4 contains the results for the $1+\varepsilon=1.5$ case. In panel (a), the quantities $\alpha(\omega)^{(\sigma,\Omega,1)}$ and $\alpha(\omega)$ are shown on a log–log plot covering three decades of the spectrum. The K–K prediction deviates noticeably from $\alpha(\omega)$ in the second decade and higher. In panel (b) $\alpha(\omega)^{(\sigma,\Omega,1)}$ and $\alpha(\omega)$ are compared linearly in the $0.001<\omega/\Omega\leqslant 0.01$ decade. Here, the correspondence is very good with a power-law fit of $1+\varepsilon=1.46$. As shown in panel (c), the Ω series term is about an order of magnitude larger than the logarithmic term, but is itself about an order of magnitude smaller than $\alpha(\omega)$. In panel (d) $\alpha(\omega)^{(\sigma,\Omega,1)}$ and $\alpha(\omega)$ are compared on a linear scale over the top decade. Similar to the two previous cases, the predicted exponent of $1+\varepsilon=1.13$ in this top decade is only about 75% of the target value. Panel (e) shows the two artifactual terms in $\alpha(\omega)^{(\sigma,\Omega,1)}$. The two terms have similar shapes although they differ in sign, and the Ω series clearly has the greater magnitude of the two. Note that the y axis in panel (e) is about a factor of 5 broader than that for panel (d).

The five panels of Fig. 5 display the results for the $1+\varepsilon=1.9$ case. In panel (a), the quantities $\alpha(\omega)^{(\sigma,\Omega,1)}$ and $\alpha(\omega)$ are shown on a log–log plot covering six decades of the spectrum up to Ω. The K–K prediction deviates from $\alpha(\omega)$ increasingly from the smallest decade up to Ω. Panel (b) shows $\alpha(\omega)^{(\sigma,\Omega,1)}$ and $\alpha(\omega)$ two decades down from the top. Here, the correspondence is not as strong as in the previous three cases, but the fit exponent of $1+\varepsilon=1.77$ for this decade accounts for 93% of the target value. For the artifact components shown in panel (c), it is clear that the Ω-series term is dominant, with no significant contribution from the log term. In panel (d) $\alpha(\omega)^{(\sigma,\Omega,1)}$ and $\alpha(\omega)$ are compared over the top decade. Here, the difference is dramatic, although the fit exponent of $1+\varepsilon=1.41$ is 74% of the target value, a similar percentage as in the other power-law cases in the top decade.

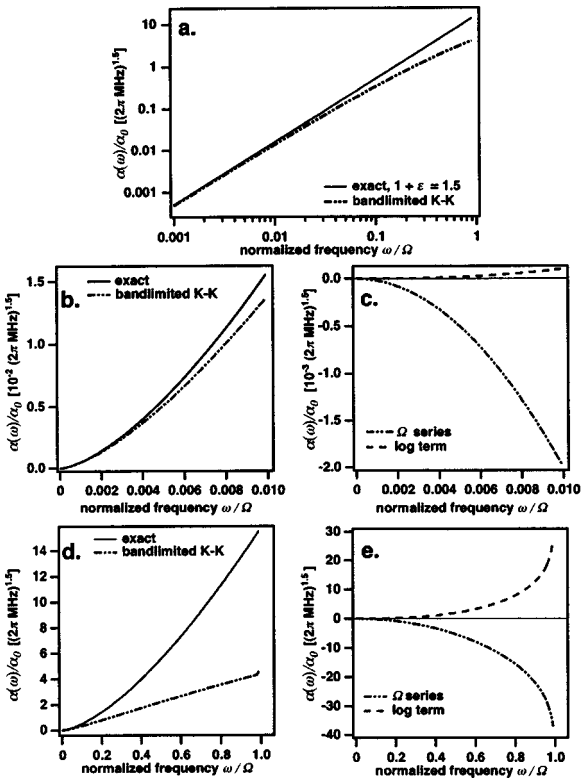

FIG. 4. (a) Log–log plot of the exact and restricted-interval once-subtracted K–K prediction for attenuation coefficient for $1+\varepsilon=1.5$. The plot covers three decades in frequency. (b) A linear plot of the exact and predicted attenuation coefficients in the third decade, $0.001<\omega/\Omega\leqslant 0.01$. (c) The two error terms, the Ω series [Eq. (16)] and the log term [Eq. (17)], in the K–K calculations for the third decade. The vertical scale is an order of magnitude smaller than that in panel (b). (d) A linear plot of the exact and predicted attenuation coefficient over the top decade ($\omega/\Omega<1.0$). (e) The two error terms in the K–K calculations over the top decade. The vertical axis is about 5 times broader than that of panel (d).

Panel (e) shows the two artifactual terms in $\alpha(\omega)^{(\sigma,\Omega,1)}$. In panel (e), the dominance of the Ω series in the artifact is clear, although the logarithmic term counterbalances it somewhat.

In each respective decade shown, the Ω series term is of a similar magnitude across the three $\varepsilon>0$ cases, while the log term provides less of a counterbalance as ε increases. To illustrate this trend, we add Eq. (16) and Eq. (17) to get the total artifact, writing the logarithm in Eq. (17) in its power series form. The first term in the total artifact series is

$$\alpha_0\omega^{1+\varepsilon}\frac{2}{\pi}\tan\left[(1+\varepsilon)\frac{\pi}{2}\right]\left(\frac{1}{1-\varepsilon}\frac{\Omega^{\varepsilon}}{\omega^{\varepsilon}}-1\right)\frac{\omega}{\Omega}. \tag{18}$$

(For $\omega<\Omega/2$, this first term approximation is accurate to better than 10%.) In the last bracket of Eq. (18), the first term is from the Ω series and the second is from the log term. The tangent can also be expanded to first order as $\tan[(1+\varepsilon)\times(\pi/2)]\approx(\varepsilon-1)(\pi/2)$ (which is accurate to better than 10% for $\varepsilon>0.66$)

$$\alpha_0\omega^{1+\varepsilon}\frac{2}{\pi}(\varepsilon-1)\frac{\pi}{2}\left(\frac{1}{1-\varepsilon}\frac{\Omega^{\varepsilon}}{\omega^{\varepsilon}}-1\right)\frac{\omega}{\Omega}$$

$$=-\alpha_0\omega^{1+\varepsilon}\left(\frac{\Omega^{\varepsilon}}{\omega^{\varepsilon}}+(\varepsilon-1)\right)\frac{\omega}{\Omega}. \tag{19}$$

As shown by the above expression, as ε increases towards 1, the log-term contribution goes to zero while the singularity in the first Ω-series term compensates for the zero in the tangent, resulting in a finite nonvanishing contribution.

The power law predicted by K–K for a given decade can be calculated using the following formula:

$$(1+\varepsilon)_k^{(\sigma,\Omega,1)}=\log_{10}\left[\frac{\alpha^{(\sigma,\Omega,1)}(10^{-k+1}\Omega,\omega_0)}{\alpha^{(\sigma,\Omega,1)}(10^{-k}\Omega,\omega_0)}\right]$$

$$=1+\varepsilon+\log_{10}\left[\frac{1+\frac{2}{\pi}\tan\left[(1+\varepsilon)\frac{\pi}{2}\right]\sum_{n=1}^{\infty}\left(\frac{10^{\varepsilon(k-1)}}{2n-\varepsilon-1}-\frac{1}{2n-1}\right)10^{(1-k)(2n-1)}}{1+\frac{2}{\pi}\tan\left[(1+\varepsilon)\frac{\pi}{2}\right]\sum_{n=1}^{\infty}\left(\frac{10^{\varepsilon k}}{2n-\varepsilon-1}-\frac{1}{2n-1}\right)10^{-k(2n-1)}}\right] \quad (0<\varepsilon<1) \tag{20a}$$

$$=1+\log_{10}\left[\frac{1-\frac{4}{\pi^2}\sum_{n=1}^{\infty}\left(\frac{1}{2n-1}\ln 10^{k-1}+\frac{1}{(2n-1)^2}\right)10^{(1-k)(2n-1)}}{1-\frac{4}{\pi^2}\sum_{n=1}^{\infty}\left(\frac{1}{2n-1}\ln 10^{k}+\frac{1}{(2n-1)^2}\right)10^{-k(2n-1)}}\right] \quad (\varepsilon=0), \tag{20b}$$

where k is a positive integer, $\omega_0\ll 10^{-k}$, and $\sigma\ll 10^{-k}\,\Omega$. Once again the logarithms in the artifact have been written in the power series form. The top decade is given by $k=1$ and the lower decades by the higher integers. In the top decade, this

formula matches the exponents numerically fit to the predicted curves to 2% and in the lower decades it matches better than 0.8%. Below the first decade (i.e., $k \geqslant 2$), the above formula is essentially determined by the first terms in the infinite series

$$(1+\varepsilon)_{k\geqslant 2}^{(\sigma,\Omega,1)} = 1+\varepsilon+\log_{10}\left[\frac{1+\frac{2}{\pi}\tan\left((1+\varepsilon)\frac{\pi}{2}\right)\left(\frac{10^{\varepsilon(k-1)}}{1-\varepsilon}-1\right)10^{(1-k)}}{1+\frac{2}{\pi}\tan\left((1+\varepsilon)\frac{\pi}{2}\right)\left(\frac{10^{\varepsilon k}}{1-\varepsilon}-1\right)10^{-k}}\right] \quad (0<\varepsilon<1), \tag{21a}$$

$$= 1+\log_{10}\left[\frac{1-\frac{4}{\pi^2}(\ln 10^{k-1}+1)10^{(1-k)}}{1-\frac{4}{\pi^2}(\ln 10^{k}+1)10^{-k}}\right] \quad (\varepsilon=0). \tag{21b}$$

As shown in this section, the restricted K–K method is clearly not practical for the prediction of power-law exponents in the $1 \leqslant 1+\varepsilon < 2$ range. Even in the most favorable case of $\varepsilon=0$, accurate predictions require the data to span a spectrum up to 50 times the lowest valid frequency in the measurement. Such wideband data are rarely available as acquiring dispersion and/or attenuation data over even a single decade in frequency is a challenging task (at least with a single set of transducers, pulsers, and amplifiers). For example, if one were interested in the attenuation behavior around 2 MHz, dispersion data would be required up to at least 100 MHz to achieve reasonable accuracy. The data would also need to extend down a decade or so below 2 MHz. A direct fit of the data to the power law model of Eq. (2) and Eq. (3) is probably the best approach as the model-independent method is so spectrally demanding.

One use of these results could be in extrapolating the range of knowledge of a system beyond the finite spectral window of our measurement system. It is possible that the power-law behavior only persists over a limited spectrum, and the system exhibits some other type of behavior elsewhere. The restricted K–K integrals could be interpreted as representing the power-law portion of the system's behavior. A successful fit of the data to the causal model within the measurement bandwidth could then indicate that the dispersion follows the model for several decades beyond the high end of the data; otherwise, the fit to the attenuation data would exhibit some deviation. The quantitative implications of this idea remain to be explored.

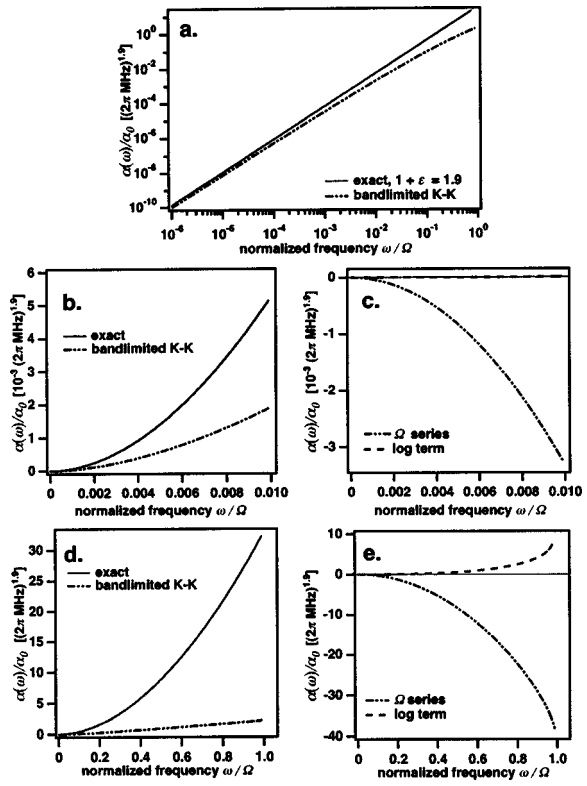

FIG. 5. (a) Log–log plot of the exact and restricted-interval once-subtracted K–K prediction for attenuation coefficient for $1+\varepsilon=1.9$. The plot covers six decades in frequency. (b) A linear plot of the exact and predicted attenuation coefficient for the third decade, $0.001<\omega/\Omega\leqslant 0.01$. (c) The two error terms, the Ω series [Eq. (16)] and the log term [Eq. (17)], in the K–K calculations for the third decade. The vertical scale is of the same order of magnitude as in panel (b). (d) A linear plot of the exact and predicted attenuation coefficients for the top decade, $\omega/\Omega<1.0$. (e) The dominant error terms in the K–K calculations for the top decade. The vertical scale is of the same order of magnitude as in panel (d).

C. On predicting dispersion from the attenuation coefficient

As shown above, in predicting the attenuation coefficient the restricted K–K relations produce the correct power-law form for both zeroth- and first subtraction orders. Even though the zeroth-order result does not converge in the $\Omega\rightarrow\infty$ limit, as the bandwidth increases the slope of the predicted attenuation does approach the correct value. When predicting the dispersion from power-law attenuation for the various orders of restricted K–K, the results are more complex in both form and interpretation. The dispersion prediction problem differs from the attenuation case in two important respects: (1) the lowest order convergent relation is the twice-subtracted form, and (2) the lower-order nonconvergent results do not produce σ- and Ω-independent terms that correspond to the correct functional form of the dispersion. The wider implications of the dispersion results within the

context of the search for a more generally applicable K–K method are yet to be explored.

V. CONCLUSION

In this work, we have demonstrated the impact of bandwidth restriction on the causal prediction of the attenuation coefficient from dispersion for power-law systems. The calculations using both the zeroth- and first-order subtracted K–K relations generate analytical results as sums of two terms. The first term is the proper power-law form for the attenuation coefficient, while the second consists of all the artifactual factors which have explicit dependencies on the limits of integration. We have shown that the once-subtracted relation converges to $\alpha(\omega)$ as the bandwidth grows to encompass larger portions of the frequency axis while the zero-order transform diverges as $\Omega \to \infty$. As illustrated in the numerical studies, the restricted K–K predictions grow more accurate as $1+\varepsilon \to 1$. The predictions are also better when the frequency scale of interest is farther removed from the upper limit of integration. The bandwidth-restricted K–K relations reveal the causal linkage between power-law attenuation and dispersion in the analytical results. In the direct application to experimental data the link may be somewhat obscured as the finite-bandwidth artifacts can be substantial. However, with the analytical expressions available in this paper it is possible to conceive of methods for correcting these results, perhaps within the context of a general model-independent approach to finite-bandwidth K–K calculations.

ACKNOWLEDGMENTS

This work is supported in part by NIH Grant No. R37 HL40302. Dr. Mobley is also supported by an appointment to the Oak Ridge National Laboratory Postdoctoral Research Associates Program administered jointly by the Oak Ridge Institute for Science and Education and Oak Ridge National Laboratory. Oak Ridge National Laboratory is managed by UT-Battelle, LLC, for the U.S. Dept. of Energy under Contract No. DE-AC05-00OR22725.

[1] J. Mobley, K. R. Waters, M. S. Hughes, C. S. Hall, J. N. Marsh, G. H. Brandenburger, and J. G. Miller, "Kramers–Kronig relations applied to finite bandwidth data from suspensions of encapsulated microbubbles," J. Acoust. Soc. Am. **108**(5), 2091–2106 (2000); **112**(2), 760–761(E) (2002).

[2] K. R. Waters, M. S. Hughes, J. Mobley, G. H. Brandenburger, and J. G. Miller, "On the applicability of Kramers–Kronig relations for ultrasonic attenuation obeying a frequency power law," J. Acoust. Soc. Am. **108**(2), 556–563 (2000).

[3] T. L. Szabo, "Causal theories and data for acoustic attenuation obeying a frequency power law," J. Acoust. Soc. Am. **97**, 14–24 (1995).

[4] F. A. Duck, *Physical Properties of Tissue: A Comprehensive Reference Book* (Academic, New York, 1990), p. 112.

[5] *Tissue Substitutes, Phantoms, and Computational Modeling in Medical Ultrasound, ICRP Report No. 61* (International Commission on Radiation Units and Measurements, Bethesda, MD, 1998), p. 8.

[6] H. M. Nussenveig, *Causality and Dispersion Relations* (Academic, New York, 1972), pp. 28–33.

[7] J. Mobley, K. R. Waters, C. S. Hall, J. N. Marsh, M. S. Hughes, G. H. Brandenburger, and J. G. Miller, "Measurements and predictions of the phase velocity and attenuation coefficient in suspensions of elastic microspheres," J. Acoust. Soc. Am. **106**(2), 652–659 (1999).